

A high-order adaptive integration method for wave propagation in range-independent fluid–solid media

Sven Ivansson and Ilkka Karasalo

Department of Hydroacoustics and Seismology, National Defence Research Establishment, S-172 90 Sundbyberg, Sweden and Department of Technical Acoustics, Royal Institute of Technology, S-100 44 Stockholm, Sweden

(Received 1 March 1991; accepted for publication 1 May 1992)

Efficient computation of the Hankel-transform integral for the wave field in a laterally homogeneous fluid–solid medium is nontrivial, since the integrand may be both oscillating and irregularly peaked. We propose a high-order, adaptive integration method suitable for integrands with these characteristics. The method combines trapezoidal or Filon sums, obtained with several step sizes, with polynomial or Bulirsch–Stoer rational extrapolation to increase the order of convergence and to obtain error estimates. This technique is combined with adaptive interval halving, maintaining a hierarchy of subintervals, meshes, and function values in a stack to eliminate duplicate function evaluations. Computational results from an underwater acoustics application are presented. At any level of accuracy, the proposed method requires less computational work than nonadaptive trapezoidal or Filon quadrature, the difference growing to orders of magnitude as the accuracy increases.

PACS numbers: 43.30.Bp, 43.30.Ma

INTRODUCTION

To date, many algorithms for range-independent media using Hankel-transform techniques have been designed, and are used routinely as analysis tools in seismo-acoustic wave propagation. Among the best known are the propagator matrix method by Thomson and Haskell^{1,2} and subsequent related methods,^{3–5} based on computing the matrizant of the system of ODEs after discretizing into horizontal layers with constant or linearly varying material parameters. A slightly different approach, with recursive updating of a reflection-coefficient matrix, was proposed by Kennett.⁶ The more recent “global matrix” algorithm by Schmidt^{7,8} discretizes the medium in a similar way, but assembles and solves a banded system of equations for the particular solutions in the layers, much like a finite element method. Conventional finite-element and finite-difference techniques are used in the codes for solid media by Alekseev and Mikhailenko,⁹ Spudich and Ascher,¹⁰ and Olson *et al.*¹¹

The performance of any algorithm based on the Hankel-transform representation, in terms of achieved accuracy versus computational effort, is strongly dependent on the numerical scheme chosen for computing the transform integrals. Several techniques are in use, including standard numerical quadrature using the fixed-step trapezoidal (Ref. 12, Sec. 7.4) and Filon¹³ rules. In the “fast field” method,¹⁴ the kernel of the Hankel-transform integral is approximated by its asymptotic form for large arguments, and the integral is then evaluated at a set of equidistant range values by the FFT algorithm. Other approaches that exploit the known analytical form of the kernel are the “fast Hankel transform” method,¹⁵ and techniques for accelerating the convergence of the truncated transform integral.^{16,17}

In general, the Hankel-transform integrand is an analytic function of horizontal wave number, with poles at the eigenvalues of a two-point boundary value problem for the system of ODEs. If a nonreflecting boundary condition is imposed, the integrand has, in addition, branch points at ω/c_p and ω/c_s , where c_p and c_s are the *P*- and *S*-wave speeds in the deepest (infinite) layer. Whenever weakly damped waveguide modes exist, their poles have small imaginary parts, making the integrand highly peaked as a function of real wave number. Correspondingly, the maximal step size Δk_{\max} at numerical quadrature, consistent with keeping the error per unit step within a preselected bound, is a strongly varying function of wavenumber k , with minima at the peaks of the integrand. Application cases where Δk_{\max} varies by several orders of magnitude over the wave-number interval of interest are not uncommon. The locations of the peaks, and thus the minima of Δk_{\max} , depend on the material and source parameters of the individual case and are not in general known *a priori*.

The above considerations suggest that the Hankel-transform integrals are well suited for computation by adaptive numerical quadrature techniques. Such techniques aim at achieving a requested overall accuracy with minimal computational work by evaluating the integrand at adaptively chosen points.^{18–20} The application of adaptive quadrature on oscillatory integrands has been studied by Xu and Mal.²¹ They propose a modified Clenshaw–Curtis scheme, combined with interval subdivision, and show that it performs well in their test cases, including a wave-number integral for a two-layered solid. The use of adaptive quadrature techniques in the present application appears not to have attracted much attention, however.

Our purpose is twofold: First, we show in Sec. II that a

high-order, adaptive quadrature scheme, suitable for the Hankel-transform integrals, may be designed by combining well-known second-order schemes with extrapolation and adaptive interval halving. Second, we present in Sec. IV numerical results from an underwater acoustics application, demonstrating the favorable performance of the adaptive method in comparison with nonadaptive low-order techniques. The improvement is significant already at modest accuracy requirements, and grows rapidly as the accuracy requirements increase. Thus, the adaptive method improves the computational economy and reliability both in routine application analyses, and in situations such as program verification where tight accuracy demands are needed, cf. the discussions in Refs. 22 and 23.

I. HANKEL REPRESENTATION OF THE FIELD IN A FLUID-SOLID MEDIUM

We consider a laterally homogeneous medium composed of fluid and solid regions, separated by horizontal interfaces. The deepest region is a homogeneous half-space. A cylindrical coordinate system (r, ϕ, z) is introduced with basis vectors $\mathbf{e}_r, \mathbf{e}_\phi, \mathbf{e}_z$, and with the z axis pointing downwards. Monofrequent energy, with angular frequency $\omega > 0$ and a horizontally symmetric radiation pattern, is emitted by a source distribution on the z axis.

The Lamé parameters $\lambda(z), \mu(z)$ and the density $\rho(z)$ of the medium are assumed to be piecewise continuous functions of z . Here, μ vanishes in fluid regions and must be bounded away from zero in solid regions. Attenuation is modeled with complex λ and μ . Omitting the factor $e^{-i\omega t}$, we denote the displacement vector by

$$\mathbf{u}(r, z) = u(r, z) \cdot \mathbf{e}_r + w(r, z) \cdot \mathbf{e}_z$$

and the traction vector acting on planes with normal \mathbf{e}_z by

$$\boldsymbol{\tau}(r, z) = \tau^r(r, z) \cdot \mathbf{e}_r + \tau^z(r, z) \cdot \mathbf{e}_z.$$

The body force per unit volume exerted by the line source is

$$\begin{aligned} \mathbf{f}(r, z) &= \nabla \left(\frac{\delta(r)}{2\pi r} \cdot g(z) \right) \\ &= \frac{\partial}{\partial r} \left(\frac{\delta(r)}{2\pi r} \right) \cdot g(z) \cdot \mathbf{e}_r + \frac{\delta(r)}{2\pi r} \cdot g'(z) \cdot \mathbf{e}_z, \end{aligned} \quad (1)$$

where the function $g(z)$ is the source density. The symmetric point source $\mathbf{f} = \nabla(\delta_{(0,0,z)})$ is obtained with $g(z) = \delta(z - z_s)$.

Define the Hankel-transform operators \mathcal{J}_m , acting on functions $h(r)$, by

$$\mathcal{J}_m h(k) = \int_0^\infty h(r) \cdot J_m(k \cdot r) \cdot r \cdot dr, \quad m = 0, 1, \quad (2)$$

where J_0 and J_1 are Bessel functions of the first kind. The operators (2) are their own inverses, see, e.g., Ref. 24, Chap. 6. Applying \mathcal{J}_1 and \mathcal{J}_0 on the basic equation system for $u(r, z)$ and $w(r, z)$ derived from Newton's second law (see, e.g., Ref. 24), one obtains

$$\begin{aligned} [\mu U' - k\mu W]' &= k^2(\lambda + 2\mu)U + k\lambda W' \\ &\quad - \rho\omega^2 \cdot U + (k/2\pi) \cdot g, \end{aligned} \quad (3)$$

$$\begin{aligned} [(\lambda + 2\mu)W' + k\lambda U]' &= k^2\mu W - k\mu U' \\ &\quad - \rho\omega^2 \cdot W - (1/2\pi) \cdot g', \end{aligned} \quad (4)$$

where $U(k, z) = (\mathcal{J}_1 u(\cdot, z))(k)$, $W(k, z) = (\mathcal{J}_0 w(\cdot, z))(k)$, and the ' denote derivatives with respect to z . The bracketed quantities in (3) and (4) are

$$T'^z(k, z) = (\mathcal{J}_1 \tau'^z(\cdot, z))(k)$$

and

$$T''^z(k, z) = (\mathcal{J}_0 \tau''^z(\cdot, z))(k),$$

respectively.

In the fluid regions, $\mu = 0$, $T'^z = 0$, and Eqs. (3) and (4) simplify to

$$\left[\frac{T'}{\rho\omega^2} \right]' = \left(\frac{k^2}{\rho\omega^2} - \frac{1}{\lambda} \right) \cdot T + \frac{g}{2\pi \cdot \lambda}, \quad (5)$$

where $T = T''^z + g/(2\pi)$.

At an interface where the medium parameters are discontinuous, the differential equations (3)–(5) are replaced by the conditions that W , T'^z , and T''^z are continuous functions of z . If the material on both sides of the interface is solid, then in addition U must be continuous there.

The medium is bounded from above by a free surface, and from below by a source-free homogeneous solid half-space. The boundary conditions are thus

$$T'^z = T''^z = 0 \text{ at the free surface,} \quad (6)$$

no upgoing P or S wave in the homogeneous solid half-space. (7)

The condition (7) can be formulated as two linear equations for U , W , T'^z , T''^z at the boundary of the homogeneous half-space.²⁴

In conclusion, the pressure field $P(r, z)$ in the fluid is given by

$$P(r, z) = -\tau^z(r, z) \quad (8)$$

$$= -\int_0^\infty T''^z(k, z) \cdot J_0(k \cdot r) \cdot k \cdot dk \quad (9)$$

$$= -\frac{1}{2} \int_{-\infty}^\infty T''^z(k, z) \cdot H_0^{(1)}(k \cdot r) \cdot k \cdot dk, \quad (10)$$

where $T''^z(k, z)$ is the solution to (5). Equation (10) follows from the fact that $T''^z(k, z)$ is even in k .

We are concerned with computing $P(r, z)$ efficiently from (9) or (10) by numerical quadrature. Since each evaluation of the integrand is computationally burdensome—the solution for a fixed k of the boundary value problem (3)–(7) is required—the quadrature scheme should use as few k values as possible to achieve a given accuracy. The adaptive quadrature method described in Sec. II was designed with this objective in mind.

We have used two different techniques for numerical solution of the boundary-value problem: a propagator-matrix method, and a finite-element method.

The propagator matrix method becomes particularly simple for the common case with one fluid region only, bounded by solid region(s), and a point source at $z = z_s$ in the fluid. The systems (3)–(4) and (5) are first rewritten as systems of first-order equations for ωU , ωW , T'^z , T''^z , and ωW , T , respectively. Certain boundary values are then pro-

pagated from below and from above, respectively, to the source level $z = z_s$. To avoid problems with numerical cancellation, certain 2×2 subdeterminants are propagated through the solid regions. For details, see Refs. 4, 5, and 25. The propagated values are matched to a source condition at $z = z_s$. A unique match is possible except for a discrete set of k : the normal modes that can be identified by the zeros of the 2×2 determinant of the matching equations.

As is common practice, the medium is discretized into layers with a simple depth dependence of the parameters.⁸ To avoid overflow during the propagation, the number of layers is partly chosen adaptively with respect to the wave number k .

In the finite element method, the boundary value problem (3)–(7) for the unknown functions $U, W, T/\omega$ is formulated as a variational problem for a symmetric bilinear integral form, cf. Ref. 26. An approximate solution is then found by restricting the variational problem to a finite-dimensional subspace of (in our case) piece-wise linear polynomials, see, e.g., Ref. 27 for details.

The FEM solution is obtained from a linear system of equations

$$\mathbf{A}(k)\mathbf{x} = \mathbf{g}(k), \quad (11)$$

where \mathbf{x} contains the unknown function values at the nodes, $\mathbf{g}(k)$ represents the source distribution, and $\mathbf{A}(k)$ is a complex, symmetric matrix with band structure. With a rigid-bottom boundary condition, $\mathbf{A}(k)$ is a quadratic polynomial as function of k . This is also true with the homogeneous solid half-space boundary condition (7), except for the lower right-hand 2×2 or 1×1 corner of $\mathbf{A}(k)$, the latter case occurring if the medium adjacent to the homogeneous half-space is fluid. Thus, by keeping the three coefficient matrices of the polynomial in store, $\mathbf{A}(k)$ may be recomputed efficiently when the value of k changes.

The equation system (11) may be solved by, e.g., standard LDL^T decomposition without pivoting. This technique is faster and more storage conserving than methods relying on pivoting, but should be combined with monitoring of element growth as a safeguard against breakdown that in theory may occur at a finite set of k values (Ref. 28, Sec. 3). However, we have not observed such breakdown in practice.

We remark that no additional assumptions, such as a small number of homogeneous layers or a point-source distribution, are required with the FEM technique. On the other hand, for simple model cases where such assumptions are justified, the propagator-matrix method is in general more efficient, cf. Ref. 29.

II. A METHOD FOR ADAPTIVE NUMERICAL QUADRATURE

In this section we describe a method for adaptive quadrature for computing the Hankel-transform integrals. The algorithm is applicable to numerical quadrature in general, but is particularly suited for integrands that may be irregularly peaked and/or oscillating with a known period. In connection with the present work, it was applied on the test cases considered by Xu and Mal,²¹ including a wave-number integral for a two-layered solid, with results roughly com-

parable with those of the modified Clenshaw–Curtis scheme proposed there.

We require that a quadrature scheme is available for computing an approximation $S(h)$ to $\int_a^b f(x)dx$ using a constant step size h . $S(h)$ is assumed to be of the form

$$S(h) = \int_a^b f(x)dx + \sum_{\nu=1}^r c_\nu h^{2\nu} + O(h^{2r+2}), \quad (12)$$

when $h \rightarrow 0$. This asymptotic form holds for approximations $S(h)$ computed by the trapezoidal as well as the Filon method, provided that f is sufficiently regular (see Ref. 12, Sec. 7.4) and the Appendix.

A well-known method to increase the order of convergence of the quadrature scheme (12) is to compute $S_0 = S(h_0), S_1 = S(h_1), \dots$ for a sequence of decreasing step sizes $h_0 > h_1 > \dots > 0$. The sequence could be chosen by step-size halving, but a more economical alternative is $h_0, h_0/2, h_0/3, h_0/4, h_0/6, h_0/8, \dots$ as suggested by Bulirsch and Stoer.³⁰ After each evaluation of an S_i , a family of polynomials or, alternatively, certain rational functions of h^2 of successively higher order are fitted to the available pairs (h_i^2, S_i) by interpolation (Ref. 31, Sec. 3.3). The extrapolated values of the interpolants at $h = 0$ are increasingly accurate estimates of the unknown value $S(0) = \int_a^b f(x)dx$. The coefficients of the interpolants need not be computed explicitly. In fact, if $S_{i,j}$ denotes the value at $h = 0$ of the interpolant to $(h_i^2, S_i), \dots, (h_{i+j}^2, S_{i+j})$, then simple recursion formulas for $S_{i,j}$ in both the polynomial and the rational case are given in Ref. 30.

The value $S_{i,j}$ may be arranged in a “rombic” extrapolation table where row index i grows with decreasing step size, and column index j grows with increasing order of extrapolation. Thus, the table grows after each evaluation of an S_i by the addition of one row at the bottom, the new elements being entered from left to right. The absolute error of $S_{i,j}$ as an approximation to $\int_a^b f(x)dx$ may be estimated by the difference

$$\Delta_{i,j} = |S_{i,j} - S_{i+1,j-1}|. \quad (13)$$

Possible alternatives are $\Delta_{i,j} = |S_{i,j-1} - S_{i+1,j-1}|$ or $\Delta_{i,j} = |S_{i,j} - S_{i,j-1}|$, where the last estimate is the most conservative.

This well-known technique for numerical quadrature is very efficient when the function $f(x)$ is equally smooth throughout the entire interval of integration. In our algorithm it is combined with adaptive interval halving, thereby extending its applicability to “peaked” functions, whose derivatives may vary by orders of magnitude in the interval (a,b) . The interval-halving strategy produces a stack of contiguous, non-overlapping subintervals $(a_1, b_1), (a_2, b_2), \dots, (a_N, b_N)$ such that

$$b_n - a_n = (b_{n-1} - a_{n-1})/2^{l_n}, \quad n = 2, 3, \dots, N, \quad (14)$$

where $l_N = 0$, l_n is a positive integer for $n < N$, and $a = a_1 < b_1 = a_2 < b_2 = a_3 \dots < b_N \leq b$. The union of the subintervals, (a, b_N) , is the portion of (a, b) where the integral is yet unknown.

The objective of the algorithm is to compute $V = \int_a^b f(x)dx$ with an absolute error not exceeding a re-

quested tolerance $\epsilon > 0$. Apart from ϵ , the values of three control parameters, I , J , and H , must be given *a priori*. No extrapolation table will be continued beyond neither row I nor column J . No entry S_{ij} is accepted as converged unless $h_{i+j} < H$. In practice we have used, e.g., $I = 9$ and $J = 7$, but the performance of the algorithm is not very sensitive to small changes of these values. H is a safety parameter, it is usually chosen guided by *a priori* information on the function.

The algorithm is composed of the following steps:

1. *Initialization:* Push the given interval (a, b) onto the subinterval stack. Initialize the accumulated value of the integral, \hat{V} , to 0.

2. *Extrapolated quadrature in a subinterval:* Set $h_0 = b_c - a_c$, where (a_c, b_c) denotes the top element of the subinterval stack, and $i = 0$. Set the absolute error bound to be used in the subinterval to

$$\epsilon_c = \frac{b_c - a_c}{b - a} * \epsilon. \quad (15)$$

(a) *Quadrature with constant step size:* Select h_i from the step-size sequence and compute $S_{i,0} = S(h_i)$ by Eq. (12).

(b) *Extrapolation and convergence check:* Add the row starting with $S_{i,0}$ to the extrapolation table using the S_{ij} recursion, observing the bound $j \leq J$. If $\Delta_{k,l} \leq \epsilon_c$ for a new value $S_{k,l}$ with $l > 0$ and if $h_i < H$, increase \hat{V} by $S_{k,l}$ and proceed to step 3.

(c) *Refine the step-size:* If $i < I$, increase i by one and go to step 2(a).

(d) *Split the subinterval:* Put $x_m = (a_c + b_c)/2$ and change the bounds of the top interval in the stack to (a_c, x_m) . Then push the interval (x_m, b_c) onto the stack, and go to step 2.

3. *Termination check after convergence in a subinterval:* Pop the subinterval stack. If the stack is nonempty, then go to step 2; otherwise terminate, accepting the current value of \hat{V} as an approximation to $V = \int_a^b f(x) dx$.

Remark 1: The same mesh point x_n is normally selected several times by different instances of the quadrature step 2(a). However, duplicate evaluations of the function value $f(x_n)$ are eliminated by keeping function values in store until they are no longer needed. The store is organized as an array accompanied by a pointer stack whose depth changes in parallel with the subinterval stack.

Remark 2: In practice, rather than storing the values S_{ij} in an extrapolation table, a similar table of the differences $S_{ij} - S_{i+1, j-1}$ is maintained for improved accuracy in the presence of rounding errors. The table need not be stored in full, since only its last row is used in the recursion in step 2(b), cf. Ref. 32.

Remark 3: If $f(x)$ is singular or sufficiently irregular at some point x_s , then the convergence test in step 2(b) fails for all subintervals containing x_s , until eventually the subinterval stack overflows, and an error exit occurs in step 2(d). Other criteria for diagnosing irregular behavior and enforcing an error exit could obviously be added in.

Remark 4: The following simple extensions of the algorithm have occasionally proved to be useful: (i) Dividing the interval (a, b) at the outset into subintervals small enough

for $h_i < H$ to hold at stack level one initially. (ii) Increasing the error bound in step 2(b) to, e.g., $\epsilon_c + 0.01\epsilon$. This amounts to relaxing the error bound (15) towards an error-per-subinterval bound at difficult portions of the interval. In this way, the sum of the local error bounds may exceed ϵ . However, the sum still provides a useful *a posteriori* estimate of an upper bound for the global error.

III. CHOICE OF INTEGRATION PATH

The functions $T^z(k, z)$ in Eqs. (9) and (10) have the following properties as functions of k for given z in the fluid: They are even in k so we may restrict our attention to $k: \text{Im}(k) \geq 0$. They are analytic in the entire k plane except for two branch cuts and a number of normal-mode poles. The two branch cuts are associated with the vertical P and S wave numbers of the homogeneous half-space. The pole locations coincide with the zeros of a certain determinant, which is an analytic function of k in the whole k plane except at the two branch cuts. The poles in the upper half-plane lie above a polygonal path composed of a segment of the real axis and two rays (cf. Fig. 3).

A sketch of the k plane with typical locations of branch points, (hyperbolic) cuts and poles is given in Fig. 1. It is interesting to note that poles away from the axes may occur even for nonattenuating media in contrast to the situation for the purely fluid case,³³ and that poles may exist in the fourth quadrant close to the real axis, see Fig. 2.

Our first-hand choice is to evaluate $P(r, z)$ using the $H_0^{(1)}$ representation (10) with, however, the tails of the integration path shifted symmetrically into the upper half-plane for faster convergence, see Fig. 3. On the nonshifted portion

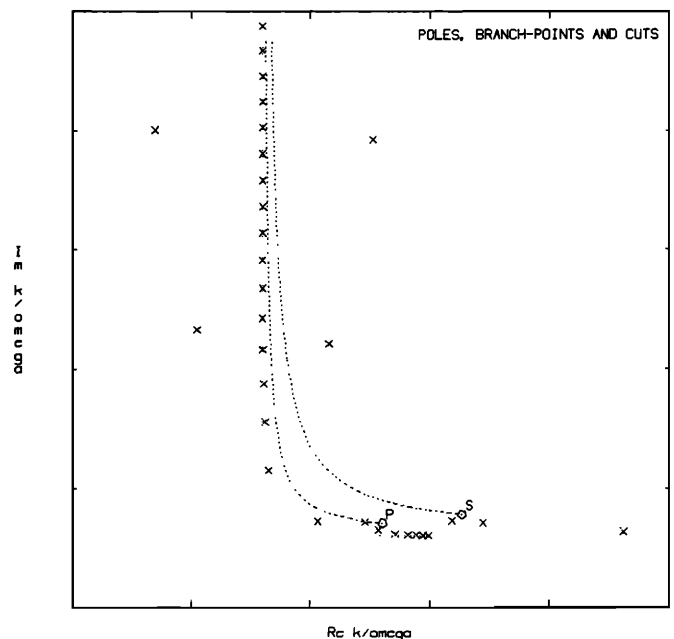


FIG. 1. Schematic plot of poles and branch points near the real axis in the upper half of the complex slowness plane. Branch-cut hyperbolas are shown by dotted lines.

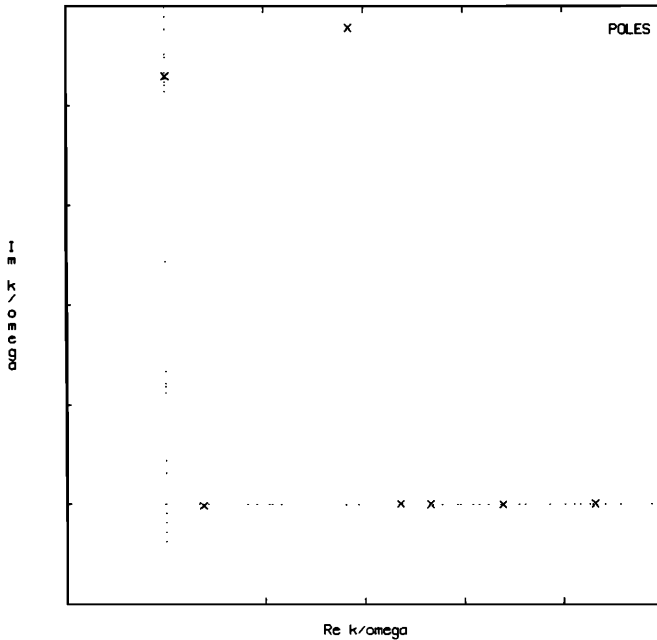


FIG. 2. Example showing a pole in the fourth quadrant very close to the real axis. The medium consists of two homogeneous layers, both with thickness 0.1 km. The top layer is a nonattenuating fluid with density 1.0 kg/dm³ and P velocity 1.5 km/s. The bottom layer is a solid with density 2.0 kg/dm³, P and S velocities 3.0 km/s and 1.8 km/s, and 0.05 dB/ λ attenuation for both P and S waves. The frequency is 22.0 Hz, and the deep boundary is assumed to be rigid.

of the path we may integrate in the right half-plane only, using the J_0 representation. We thus obtain the following alternative to (9) and (10)

$$\begin{aligned}
 P(r,z) = & - \int_{\Gamma_0} T^{zz}(k,z) \cdot J_0(k \cdot r) \cdot k \cdot dk \\
 & - \frac{1}{2} \int_{\Gamma_1} T^{zz}(k,z) \cdot H_0^{(1)}(k \cdot r) \cdot k \cdot dk \\
 & + \frac{1}{2} \int_{\Gamma_2} T^{zz}(k,z) \cdot H_0^{(1)}(k \cdot r) \cdot k \cdot dk, \quad (16)
 \end{aligned}$$

where Γ_0 is the interval $(0, k_b)$ of the real axis, and the tails Γ_1 and Γ_2 are rays extending from $\pm k_b$ into the first and

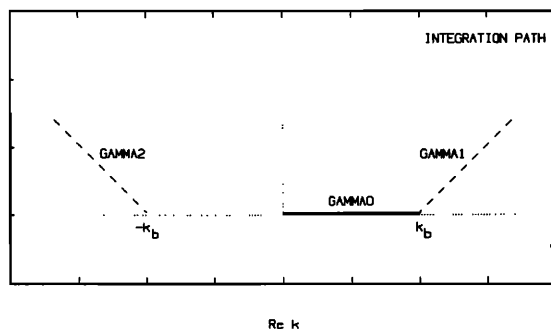


FIG. 3. Integration path, composed of the line segments Γ_0 , Γ_1 , and Γ_2 , in the complex wave-number plane.

second quadrants, respectively. The breakaway points, $\pm k_b$, must be such that no poles are located between the real axis and the shifted path. We have no completely satisfactory way of choosing k_b , however in practice a safe choice seems to be, e.g., twice the maximum wave number of the medium with the directions of the tails chosen to $\pi/4$ and $3\pi/4$, respectively. The integrand dies off exponentially along Γ_1 and Γ_2 and thus, in practice, the work for computing the last two integrals of (16) is negligible.

If poles on or very close to the real axis exist, the integrand will be singular or highly peaked on Γ_0 . Moving the path away from such poles makes the integrand smoother, cf. Ref. 8. Changes of the integration path must be done with care, however. No pole in the fourth quadrant must be enclosed unless its residue contribution is accounted for. Furthermore, the path cannot be moved too far from the real axis since $J_0(kr)$ will then increase exponentially and overflow or harmful cancellation may occur. Also, the computation of the Bessel function is less efficient for complex-valued than for real-valued arguments.

A valuable option, easily incorporated into the integration algorithm described in Sec. II, is to adjust the integration path Γ_0 into the fourth quadrant locally, with adaptive control of the adjustments. Under this option, such adjustment is triggered if the convergence test in step 2(b) of the algorithm fails and $h_i < H_a$, where h_i is the current step size and H_a is a pre-selected bound. Then, the algorithm simply records the current subinterval (a_c, b_c) for later treatment and proceeds to step 3 as if the integration over the subinterval was successful with a zero result. In this way, the delicate way of building up the stacks of calculated function values etc. is not disturbed. The function evaluations already performed for the subinterval in question are lost, however. After completing the integral along Γ_0 in this way, the recorded subintervals are processed in a second pass. First, subintervals with a common endpoint are joined. Then the integrals over the resulting (larger) subintervals are computed, again using the algorithm of Sec. 3 but now following a suitable roundabout path in the fourth quadrant. A simple choice for this path is the sloping sides of a uniform downward-pointing triangle whose base is the subinterval on the real axis. For additional safety, we optionally check that no pole was enclosed by the path adjustment, by computing the argument variation of the analytic determinant referred to above.

IV. A NUMERICAL EXAMPLE

In this section we demonstrate the efficiency of the adaptive method described in Sec. II for computing the integrals in (16). Our example case is a model of sound propagation in shallow water, with material data obtained from a location in the Baltic Sea under summer conditions.

The medium consists of a water column with depth 100 m on top of a homogeneous sediment layer with thickness 15 m. The sediment is bounded from below by rock, modeled as a homogeneous solid half-space. The material data in the sediment and the rock are

	Sediment	Rock
density (kg/dm ³)	1.3	2.62 ,
<i>P</i> velocity (km/s)	1.460	4.000,
<i>S</i> velocity (km/s)	0.834	2.309,
<i>P</i> attenuation (dB/λ)	0.30	0.36 ,
<i>S</i> attenuation (dB/λ)	0.68	0.81 .

The compressional sound-speed profile in the water and sediment is shown in Fig. 4. The boundary value problem (3)–(7) was solved with the propagator-matrix code, and hence the water column was discretized into 11 layers, in each of which the squared inverse sound velocity varies linearly with depth. The sound field is excited by a point source with frequency 50 Hz at depth 50 m.

In the middle frame of Fig. 5, we show the location of branch points, branch cuts, and poles closest to the positive real axis in the complex slowness plane. In contrast to Fig. 1, vertical branch cuts are used. The corresponding poles are more related to the behavior of T^{zz} on the real axis than are those obtained with the hyperbolic cuts, since the hyperbolas follow part of the real axis very closely. The pole locations—the zeros of the propagator determinant—were determined by a zero-finder routine based on the argument principle, adaptive halving of axis-parallel rectangles, and secant iterations for faster final convergence. Due to the branch cuts, the determinant is a four-valued analytic function, and hence proper care must be taken to select zeros on the desired Riemann sheet only. The end point of Γ_0 in Eq. (16) was chosen to $k_b = 2 \cdot 2\pi \cdot 50 \text{ km}^{-1}$.

The top frame of Fig. 5 shows $|k \cdot T^{zz}(k, z)|$ as a function of k at depth $z = 40 \text{ m}$, for k values on Γ_0 . As expected, peaks appear at the poles nearest the real axis shown in the middle frame. The main peak occurs close to the third of these poles (counted by decreasing real part). This pole is actually the wave number of the fundamental mode of the water layer, a mode whose amplitude maximum roughly coincides with the source depth. Note that no visible peaks occur at the first two poles. The energy of these modes is essentially confined to the water–sediment interface (mode 1, a Scholte mode) and the sediment (mode 2) and they are thus barely excited by a source at a depth of 50 m. The last two poles correspond to “leaking modes,”³⁴ they do not appear on the Riemann

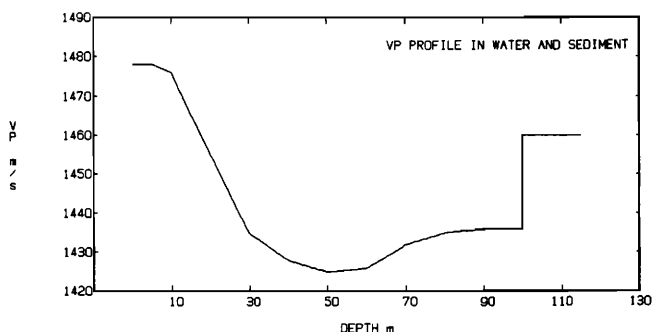


FIG. 4. Compressional wave-speed profile in the water column and sediment used in the test example.

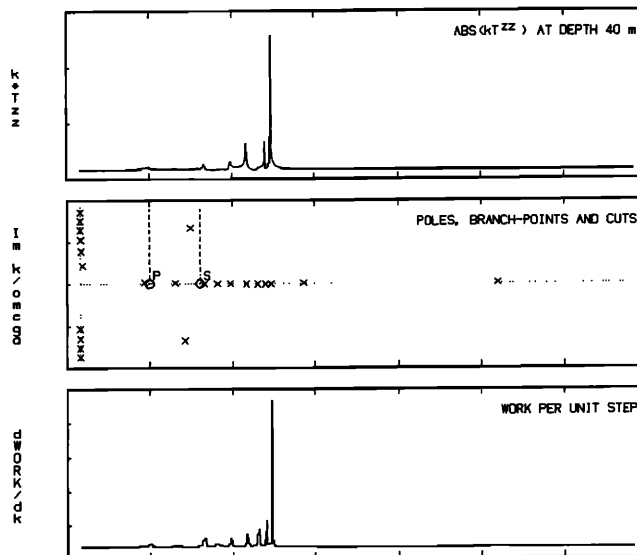


FIG. 5. Top: $|k \cdot T^{zz}(k, z)|$ at depth $z = 40 \text{ m}$ as function of real slowness. Middle: Branch points, vertical branch cuts, and corresponding poles near the positive real axis in the complex slowness plane. Bottom: Computational work/unit step with adaptive integration as function of real slowness (Filon quadrature, a short-range case).

sheet defined by the hyperbolic cuts. Thus, there are nine propagating modes in this example.

Three groups of ten equi-spaced range values in each were used for the test runs:

Short range

$$r = 0.050, 0.100, 0.150, \dots, 0.500 \text{ km},$$

Medium range

$$r = 5.550, 5.600, 5.650, \dots, 6.000 \text{ km},$$

Long range

$$r = 29.550, 29.600, 29.650, \dots, 30.000 \text{ km}.$$

For each range value, ten depth values $z = 10, 20, \dots, 100 \text{ m}$ were selected. All 10×10 complex pressure values, corresponding to the (range, depth) value pairs of a range group, were computed in the same run of the integration algorithm of Sec. II. For this purpose, the algorithm was modified to matrix-valued functions f in a straightforward way. Notice that the matrix-valued integrand is here the outer product of two vectors, which reduces the workspace needed for the stacks. The bottom frame of Fig. 5 shows a distribution of the density of the k values selected by the adaptive integration algorithm in a typical run. As expected, the k values are concentrated close to the peaks of $k \cdot |T^{zz}|$.

Four integration methods were used in the test runs: Fixed-step trapezoidal (FT), fixed-step trapezoidal Filon (FF), adaptive trapezoidal (AT), and adaptive trapezoidal Filon (AF). For each of the three range groups, the test runs were carried out as follows: First, the 10×10 complex pressure matrix was evaluated very accurately using the adaptive Filon integration method with a tight accuracy requirement. Then, each integration method was re-run repeatedly with different accuracy requirements (for the adaptive methods)

or step sizes (for the fixed-step methods) to obtain an error versus work curve. A "work" unit is defined as solving the boundary-value problem (3)–(7) once, and "error" is the largest of the relative errors of the 10×10 complex pressure values.

The error versus work curves can be found in Fig. 6. For the adaptive methods, rational extrapolation was used and the step-size bound H of Sec. II was set to guarantee at least 1.1 mesh points per asymptotic Bessel-function period. The bounds I and J of the size of the extrapolation tables were chosen to 8 and 7, respectively, and the local error bound ϵ_c was relaxed as described in Remark 4 (ii) in Sec. II. The option to adjust the integration path adaptively was not used.

The most conspicuous result in Fig. 6 is the excellent performance of the adaptive methods. In the short-range case, when two or more correct digits are desired, these methods are more than ten times as efficient as the fixed-step methods. By doubling the computational work, about five additional correct digits are obtained (this is actually expected in view of the value 7 for the parameter J). As the range increases, the gains are still impressive but smaller, since $T^{zz}(k, z)$ is smoother relative to the oscillations of the Bessel function. For the same reason, in the short range case the error versus work curves of trapezoidal Filon and ordinary trapezoidal quadrature are nearly equal, whereas Filon quadrature becomes more and more favourable as the range increases.

As should be expected, the slope of the error versus work curves of the fixed-step methods tends asymptotically to -2 as the work increases, i.e., as the step size tends to

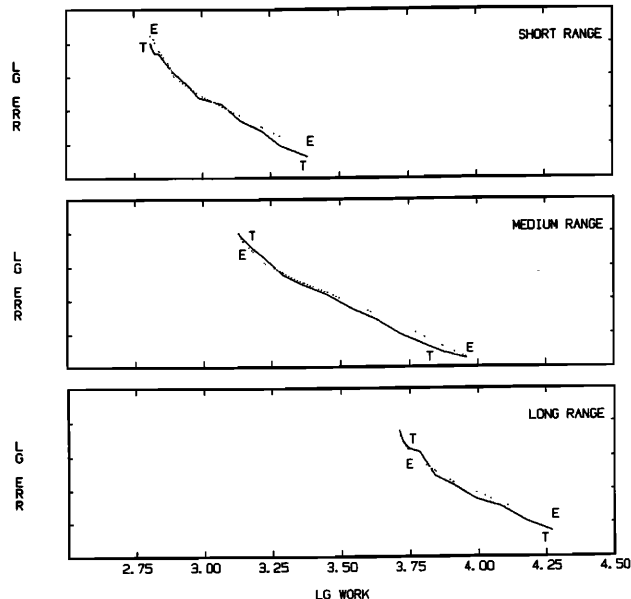


FIG. 7. Plot of $^{10}\log(\text{true relative error})$ (T), and $^{10}\log(\text{estimated upper bound of relative error})$ (E), as a function of $^{10}\log(\text{nr of work units})$ for adaptive Filon quadrature. *Top*: Short range. *Middle*: Medium range. *Bottom*: Long range.

zero. It is interesting to note that fixed-step Filon quadrature is in this example preferable to fixed-step trapezoidal quadrature for very coarse accuracy requirements only. In particular, Filon quadrature shows the larger error of the two fixed-step methods asymptotically as the step size decreases. A brief discussion of this observation, in terms of a simple test function, is given in the Appendix.

The effect of some alternative choices of the options and control parameters of the adaptive method were investigated in repeated runs of the cases in Fig. 6. Two observations from these runs are:

(i) For moderate accuracy requirements, the work needed can be reduced to about one third by relaxing the safety requirement of at least 1.1 mesh points per asymptotic Bessel-function period. For tight accuracy requirements, however, such relaxation may impair the efficiency.

(ii) Rational extrapolation performs better than polynomial extrapolation, the latter alternative may be twice as expensive in terms of work needed for a specified accuracy.

Finally we recall that Fig. 6 shows the true relative error, obtained by computing a very accurate solution in advance. In practice such a solution is not available, but the adaptive integration routine still provides an estimate of the error, cf. Remark 4 (ii) in Sec. II. In Fig. 7 we show a comparison of estimated and true relative errors as functions of computational work, for the adaptive Filon quadrature cases of Fig. 6. As can be seen, the reliability of the error estimates seems to be satisfactory.

V. CONCLUSIONS

We have described a method for computing the wave-number integrals of range-independent fluid–solid media by adaptive quadrature. The method uses trapezoidal or trape-

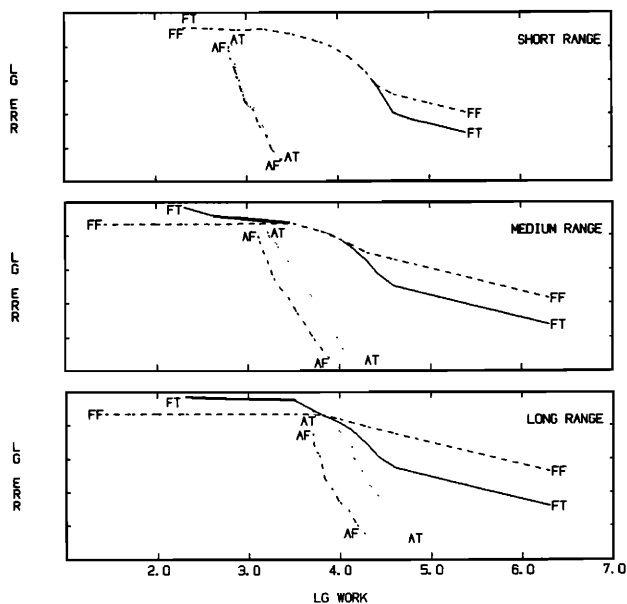


FIG. 6. Plot of $^{10}\log(\text{relative error})$ as a function of $^{10}\log(\text{nr of work units})$ for fixed-step trapezoidal (FT), fixed-step Filon (FF), adaptive trapezoidal (AT), and adaptive Filon (AF) quadrature. *Top*: Short range. *Middle*: Medium range. *Bottom*: Long range.

zoidal Filon quadrature schemes repeatedly with several step sizes, in combination with polynomial or rational extrapolation and adaptive interval halving.

The favorable performance of the proposed method, in comparison with traditional fixed-step quadrature techniques, was demonstrated in a sample case of sound propagation in shallow water. Significant gains were obtained, for the trapezoidal as well as the trapezoidal Filon scheme. The Filon scheme proved very useful in connection with the adaptive method but not, interestingly enough, in connection with the fixed-step technique. The gains observed are significant at any meaningful level of accuracy, but they are increasingly pronounced as the accuracy requirements increase. By increasing the computational work by a factor of 2, about five additional correct digits were obtained. Thus, the proposed method is useful also when a very high accuracy is needed, e.g., for the purpose of program verification or benchmark runs.

With adaptive integration, the computational work along the integration path is concentrated where it is needed. In this way, the need to smooth the integrand by shifting the path away from the real axis is reduced. When local deviations of the path are necessary, they can be done adaptively in a straightforward way.

ACKNOWLEDGMENT

We thank Rainer Kind for providing a copy of his reflectivity program for computing synthetic surface seismograms. This program was a good starting point for our work with the propagator method.

APPENDIX: FILON QUADRATURE IN THE CONTEXT OF EXTRAPOLATION

From the properties of the Bessel function J_0 follows that the integrand in Eq. (9) can be decomposed to

$$f(x) = g_1(x) \cdot e^{\gamma x} + g_2(x) \cdot e^{-\gamma x}, \quad (\text{A1})$$

where $x = k$, $\gamma = ir$, and g_1 and g_2 are (except at poles of the integrand) slowly varying functions of x in comparison to the exponential factors when γ is large. In the sequel we restrict ourselves, without loss of generality, to the basic case

$$V = \int_a^b f(x) dx = \int_a^b g(x) e^{\gamma x} dx, \quad (\text{A2})$$

where a and b are real.

In Filon's method, the function g (rather than f itself) is approximated by piecewise polynomial interpolation, and the resulting function is integrated analytically.^{13,35-39} Piecewise linear interpolation on an equi-distant mesh with step size $h = (b - a)/n$ gives the "trapezoidal Filon" estimate

$$F_T(h) = T(h) \cdot \left(\frac{\cosh(\gamma h) - 1}{(\gamma h)^2/2} \right) + \frac{f(a) - f(b)}{2} \cdot \left(h \cdot \frac{\sinh(\gamma h) - \gamma h}{(\gamma h)^2/2} \right), \quad (\text{A3})$$

where

$$T(h) = h \cdot \left(\frac{f(a) + f(b)}{2} + \sum_{j=1}^{n-1} f(a + j \cdot h) \right) \quad (\text{A4})$$

is the ordinary trapezoidal sum. If $f(x)$ is sufficiently regular, then (Ref. 12, Sec. 7.4)

$$T(h) = V + \sum_{v=1}^r A_v \cdot h^{2v} + O(h^{2r+2}), \quad (\text{A5})$$

where $A_v = \alpha_v (f^{(2v-1)}(b) - f^{(2v-1)}(a))$ for some constant α_v . Since the bracketed expressions in (A3) can be expanded in even powers of h , we immediately obtain

$$F_T(h) = V + \sum_{v=1}^r B_v \cdot h^{2v} + O(h^{2r+2}), \quad (\text{A6})$$

where B_v is a linear combination of $f^{(l)}(b) - f^{(l)}(a)$ of orders $l = 0, 1, 3, \dots, 2v - 1$. Thus the trapezoidal Filon scheme, as well as the ordinary trapezoidal scheme, has the asymptotic form required by the adaptive algorithm, cf. Eq. (12).

In the general case, we cannot expect extrapolation based on (A6) to work unless $|\gamma h|$ is small and the expansion (A5) is meaningful. In the typical case of a large imaginary γ , however, extrapolation may not be needed since $F_T(h)$ can be very accurate even if these conditions are not satisfied. By partially integrating in (A2) twice over each grid step, choosing the integration constants appropriately, and summing over grid steps [cf. the proof of (A5) in (Ref. 12, Sec. 7.4)], we obtain

$$F_T(h) = V - h^2 \cdot \int_0^1 \left(h \cdot \sum_{j=1}^n e^{\gamma \cdot x_j - 1} \cdot g^{(2)}(x_{j-1} + h \cdot t) \right) \cdot K_2(t) \cdot dt, \quad (\text{A7})$$

where $x_j = a + j \cdot h$ and

$$K_2(t) = \frac{e^{\gamma h t} - 1 - (e^{\gamma h} - 1) \cdot t}{(\gamma h)^2}. \quad (\text{A8})$$

Analogous error formulas for Filon's original formulation are given in Ehrenmark.⁴⁰ By (A7) and (A8), if γ is purely imaginary, then $|F_T(h) - V| \leq 3(b - a)G_2/|\gamma|^2$, where G_2 is the maximum of $|g^{(2)}(x)|$ in $a \leq x \leq b$.

It is interesting to note that if $h = 2m\pi i/\gamma$ where m is an integer, then $F_T(h)$ is actually independent of h . For such h , (A3) simplifies to

$$F_T(h) = \frac{f(b) - f(a)}{\gamma}, \quad (\text{A9})$$

which has the error $1/\gamma^2 \cdot \int_a^b g'(x) e^{\gamma x} dx$ as is seen by partially integrating (A2) once, cf. the paper by Fosdick.⁴¹ If by chance several such h were used in step 2 of the algorithm in Sec. II then, since $F_T(h)$ is independent of h , there is a risk (although small) of obtaining a false small or zero error estimate, and hence accepting convergence prematurely. This risk is eliminated if the parameter H is chosen so that $|\gamma H| < 2\pi$ holds. The gain in efficiency with the Filon approach is nevertheless substantial, since the ordinary trapezoidal method would hardly do with less than ten (say) points per period.

From the fixed-step cases of Fig. 6 it is apparent that $|B_1| > |A_1|$ may hold for the error constants in Eqs. (A5) and (A6). Some insight into this behavior is gained by considering (A2) but with

$$f(x) = e^{\lambda x} \cdot (e^{\gamma x} + e^{-\gamma x}), \quad (\text{A10})$$

where λ and γ are imaginary constants. Then

$$12 \cdot A_1 = (\lambda + \gamma) \cdot D_1 + (\lambda - \gamma) \cdot D_2, \quad (\text{A11})$$

$$12 \cdot B_1 = \frac{(\lambda + \gamma) \cdot D_1}{(1 + \theta)^2} + \frac{(\lambda - \gamma) \cdot D_2}{(1 - \theta)^2}, \quad (\text{A12})$$

where $\theta = \gamma/\lambda$ and

$$D_1 = e^{(\lambda + \gamma)b} - e^{(\lambda + \gamma)a},$$

$$D_2 = e^{(\lambda - \gamma)b} - e^{(\lambda - \gamma)a}.$$

Consider A_1 and B_1 as functions of λ for a fixed γ . If $|\lambda| \ll |\gamma|$, then $|\theta| \gg 1$ and thus $|B_1| \ll |A_1|$, i.e., the Filon scheme is advantageous as expected. In the other extreme, $|\lambda| \gg |\gamma|$, the methods become equivalent, as they should. For $|\lambda| \approx |\gamma|$, however, $|B_1|$ can be much larger than $|A_1|$ provided that $|\gamma(b - a)| \gg 1$ holds. (Actually things are more complicated since $|A_1|$ and $|B_1|$ are oscillatory functions. Our statement refers to the amplitudes of these oscillations.)

By Fourier theory, these observations carry over to integrands of the more general form $g(x)(e^{\gamma x} + e^{-\gamma x})$. If $g(x)$ has poles sufficiently close to the real axis, its Fourier spectrum will be broad enough to include an interval around γ . Then, provided that $|\gamma(b - a)| \gg 1$ holds, the error of the constant-step trapezoidal Filon formula may exceed that of the constant-step trapezoidal rule. The adaptive method is capable of preventing this situation by splitting the interval into parts in such a way that the $\{(b - a), \gamma, \lambda\}$ region unfavorable for the Filon scheme is avoided.

¹W. T. Thomson, "Transmission of elastic waves through a stratified solid," *J. Appl. Phys.* **21**, 89–93 (1950).

²N. A. Haskell, "The dispersion of surface waves in multilayered media," *Bull. Seismol. Soc. Am.* **43**, 17–34 (1953).

³D. G. Harkrider, "Surface waves in multilayered elastic media, 1. Rayleigh and Love waves from buried sources in a multilayered elastic half-space," *Bull. Seismol. Soc. Am.* **54**, 627–679 (1964).

⁴H. Takeuchi and M. Saito, "Seismic surface waves," in *Seismology: Surface Waves and Earth Oscillations*, Methods in Computational Physics, Vol. 11, edited by B. A. Bolt (Academic, New York, 1972).

⁵R. Kind, "The reflectivity method for a buried source," *J. Geophys.* **44**, 603–612 (1978).

⁶B. L. N. Kennett, "Reflections, rays, and reverberations," *Bull. Seismol. Soc. Am.* **64**, 1685–1696 (1974).

⁷H. Schmidt and F. Jensen, "A full wave solution for propagation in multilayered viscoelastic media with application to Gaussian beam reflection at fluid-solid interfaces," *J. Acoust. Soc. Am.* **77**, 813–825 (1985).

⁸H. Schmidt, "SAFARI, Seismo-Acoustic Fast field Algorithm for Range-Independent environments," SAFLANTCEN Report SR-113 (September 1988).

⁹A. S. Alekseev and B. G. Mikhailenko, "The solution of dynamic problems of elastic wave propagation in inhomogeneous media by a combination of partial separation of variables and finite-difference methods," *J. Geophys.* **48**, 161–172 (1980).

¹⁰P. Spudich and U. Ascher, "Calculation of complete theoretical seismograms in vertically varying media using collocation methods," *Geophys. J. R. Astron. Soc.* **75**, 101–124 (1983).

¹¹A. H. Olson, J. A. Orcutt, and G. A. Frazier, "The discrete wavenumber/finite element method for synthetic seismograms," *Geophys. J. R. Astron. Soc.* **77**, 421–460 (1984).

¹²G. Dahlquist, Å. Björck, and N. Anderson, *Numerical Methods* (Prentice-Hall, Englewood Cliffs, NJ, 1974).

¹³L. N. G. Filon, "On a quadrature formula for trigonometric integrals," *Proc. R. Soc. Edinburgh* **49**, 38–47 (1929).

¹⁴F. R. Di Napoli, "Fast field program for multilayered media," NUSC Technical Report 4103, Naval Underwater Systems Center (1971).

¹⁵W. L. Anderson, "Computation of Green's tensor integrals for three-dimensional electromagnetic problems using fast Hankel transforms," *Geophysics* **49**, 1754–1759 (1984).

¹⁶P. Cornille, "Computation of Hankel transforms," *SIAM Rev.* **14**, 278–285 (1972).

¹⁷A. D. Chave, "Numerical integration of related Hankel transforms by quadrature and continued fraction expansion," *Geophysics* **48**, 1671–1686 (1983).

¹⁸D. Kahaner and J. Stoer, "Extrapolated adaptive quadrature," *SIAM J. Sci. Stat. Comput.* **4**, 31–44 (1983).

¹⁹J. R. Rice, "A metaalgorithm for adaptive quadrature," *J. Assoc. Comput. Mach.* **22**, 61–82 (1975).

²⁰E. de Doncker, "An adaptive extrapolation algorithm for automatic integration," *SIGNUM Newsletter* **13**, 189–198 (1978).

²¹P. Xu and A. K. Mal, "An adaptive integration scheme for irregularly oscillatory functions," *Wave Motion* **7**, 235–243 (1985).

²²L. B. Felsen, "Benchmarks: An option for quality assessment," *J. Acoust. Soc. Am.* **87**, 1497–1498 (1990).

²³F. B. Jensen and C. M. Ferla, "Numerical solutions of range-dependent benchmark problems in ocean acoustics," *J. Acoust. Soc. Am.* **87**, 1499–1510 (1990).

²⁴K. Aki and P. G. Richards, *Quantitative Seismology* (Freeman, San Francisco, 1980), Vol. 1.

²⁵T. H. Watson, "A note on fast computation of Rayleigh wave dispersion in the multilayered elastic half-space," *Bull. Seismol. Soc. Am.* **60**, 161–166 (1970).

²⁶L. G. Olson and K. -J. Bathe, "Analysis of fluid-structure interactions. A direct symmetric coupled formulation based on the fluid velocity potential," *Comput. Structures* **21**, No. 1/2, 21–32 (1985).

²⁷C. Johnson, "Numerical solutions of partial differential equations by the finite element method," *Studentlitteratur*, Lund (1987).

²⁸B. N. Parlett, *The Symmetric Eigenvalue Problem* (Prentice-Hall, Englewood Cliffs, NJ, 1980).

²⁹M. Korn and G. Muller, "Comparison of the Alekseev–Mikhailenko method and the reflectivity method," *Geophys. J. R. Astron. Soc.* **72**, 541–556 (1983).

³⁰R. Bulirsch and J. Stoer, "Fehlerabschätzungen und Extrapolation mit rationalen Funktionen bei Verfahren vom Richardson-Typus," *Num. Math.* **6**, 413–427 (1964).

³¹J. Stoer, *Einführung in die Numerische Mathematik I* (Springer-Verlag, Berlin, 1972).

³²R. Bulirsch and J. Stoer, "Numerical treatment of ordinary differential equations by extrapolation methods," *Num. Math.* **8**, 1–13 (1966).

³³S. Ljunggren, "Line mobilities of infinite plates," *J. Acoust. Soc. Am.* **86**, 1419–1431 (1989).

³⁴R. A. W. Haddon, "Response of an oceanic wave guide to an explosive point source using leaking modes," *Bull. Seismol. Soc. Am.* **77**, 1804–1822 (1987).

³⁵Y. L. Luke, "On the computation of oscillatory integrals," *Proc. Cambridge Philos. Soc.* **50**, 269–277 (1954).

³⁶E. A. Flinn, "A modification of Filon's method of numerical integration," *J. Assoc. Comput. Mach.* **7**, 181–184 (1960).

³⁷E. O. Tuck, "A simple Filon-Trapezoidal rule," *Math. Comp.* **21**, 239–241 (1966).

³⁸A. I. van de Vooren and H. J. van Linde, "Numerical calculation of integrals with strongly oscillating integrand," *Math. Comp.* **20**, 232–245 (1966).

³⁹S. Mallick and N. N. Frazer, "Practical aspects of reflectivity modeling," *Geophysics* **52**, 1355–1364 (1987).

⁴⁰U. T. Ehrenmark, "On the error term of the Filon quadrature formulae," *BIT* **27**, 85–97 (1987).

⁴¹L. D. Fosdick, "A special case of the Filon quadrature formula," *Math. Comp.* **22**, 77–81 (1968).